HYDROLOGICAL PROCESSES
Hydrol. Process. **24**, 2983–2994 (2010)
Published online 29 May 2010 in Wiley Online Library
(wileyonlinelibrary.com) DOI: 10.1002/hyp.7709

Influence of pore size and geometry on peat unsaturated hydraulic conductivity computed from 3D computed tomography image analysis

F. Rezanezhad,[1,2]* W. L. Quinton,[1] J. S. Price,[2] T. R. Elliot,[3] D. Elrick[3] and K. R. Shook[4]

[1] *Cold Regions Research Centre, Wilfrid Laurier University, Waterloo, Ontario, Canada N2L 3C5*
[2] *Department of Geography, University of Waterloo, Waterloo, Ontario, Canada N2L 3G1*
[3] *Department of Land Resource Science, University of Guelph, Guelph, Canada N1G 2W1*
[4] *Centre for Hydrology, University of Saskatchewan, Saskatoon, Canada S7N 5C8*

Abstract:

In organic soils, hydraulic conductivity is related to the degree of decomposition and soil compression, which reduce the effective pore diameter and consequently restrict water flow. This study investigates how the size distribution and geometry of air-filled pores control the unsaturated hydraulic conductivity of peat soils using high-resolution (45 μm) three-dimensional (3D) X-ray computed tomography (CT) and digital image processing of four peat sub-samples from varying depths under a constant soil water pressure head. Pore structure and configuration in peat were found to be irregular, with volume and cross-sectional area showing fractal behaviour that suggests pores having smaller values of the fractal dimension in deeper, more decomposed peat, have higher tortuosity and lower connectivity, which influences hydraulic conductivity. The image analysis showed that the large reduction of unsaturated hydraulic conductivity with depth is essentially controlled by air-filled pore hydraulic radius, tortuosity, air-filled pore density and the fractal dimension due to degree of decomposition and compression of the organic matter. The comparisons between unsaturated hydraulic conductivity computed from the air-filled pore size and geometric distribution showed satisfactory agreement with direct measurements using the permeameter method. This understanding is important in characterizing peat properties and its heterogeneity for monitoring the progress of complex flow processes at the field scale in peatlands. Copyright © 2010 John Wiley & Sons, Ltd.

KEY WORDS pore size and geometry of peats; unsaturated hydraulic conductivity; X-ray computed tomography; decomposition; compressibility

Received 6 October 2009; Accepted 18 March 2010

INTRODUCTION

There is limited knowledge of the water transmission and storage properties of unsaturated peat, which plays a critical role in the hydrological cycle by linking the water table to the overlying atmosphere. For example, inadequate understanding and mathematical process description of unsaturated moisture flow to the ground surface through non-vascular, unsaturated plant tissues, have led to unreliable predictions of peat surface wetness and associated fluxes of evaporation and sensible heat (Waddington *et al*., 2009), and thus carbon (Strack and Price, 2009). Similarly, inadequate understanding and description of the interaction between water flow and storage in unsaturated peat have hindered hydrological model prediction of infiltration, drainage and water table response to rainfall and snowmelt input (Quinton and Marsh, 1999; Carey and Woo, 2001; Price and Whittington, 2010). An improved understanding of water flow and storage in unsaturated peat is therefore needed so that the key processes can be appropriately described in Land Surface Process (LSP) and other predictive models.

Peat has relatively large pores (Hayward and Clymo, 1982) that are highly inter-connected (Quinton *et al*., 2009), and total porosity often exceeds 90% (Boelter, 1968). Furthermore, the plant tissues contain closed and dead-end pores that do not conduct water, and this inactive porosity (Hoag and Price, 1997) can store up to 20% of the soil moisture. The saturated hydraulic conductivity of peat is strongly depth dependent, often decreasing by three or more orders of magnitude between the ground surface and 0·5 m below where the active porosity typically decreases from 80% near the ground surface to <50% in well-humified peat (Boelter, 1965; Hoag and Price, 1995; Quinton *et al*., 2000; Beckwith *et al*., 2003). Although, some studies report that layering of peat and other factors gives a more complicated relation between hydraulic conductivity and depth (e.g. Beckwith *et al*., 2003). Quinton *et al*. (2008) demonstrated that the reduction in hydraulic conductivity can be explained by the reduction in the size and hydraulic radius of pores with depth, as they are more decomposed and become compressed by overlying sediment, therefore imposing greater resistance to flow. However, given the very large total porosity of peat, its saturated storage and transmission properties are dramatically altered when the peat drains, limiting the extent to which the properties of

* Correspondence to: F. Rezanezhad, Department of Geography, University of Waterloo, Waterloo, Ontario, Canada N2L 3G1.
E-mail: frezanez@uwaterloo.ca

unsaturated peat can be inferred from the saturated regime (Price *et al*., 2008).

Numerous studies have considered the degree of decomposition of peat, but few have reported quantitative comparisons with other physical properties. Peat is very compressible due to its high porosity (Hobbs, 1986; Price and Schlotzhauer, 1999; Price *et al*., 2005) but also varies according to its physical properties and structure (as described above) associated with its stage of decomposition. Undecomposed peat has relatively large pores and good elastic and plastic deformation properties (high compressibility) compared with decomposed peat that has smaller pores and a higher proportion of solids (lower compressibility). Hence, peat layers are anisotropic and have a very pronounced horizontal laminar structure (Colley *et al*., 1950; Boelter, 1965; Beckwith *et al*., 2003).

Karamanev *et al*. (1994) suggested that the nature of water flow and transport through peat depends on the flow velocity because of its fractal nature, which can be quantified by the fractal dimension D (Mandelbrot, 1983), that characterizes soil-pore microstructure (Wong *et al*., 1986; Cohen, 1987; Schlueter *et al*., 1997; Xu and Sun, 2002; Xu, 2004). In this study, we used the fractal dimension to characterize pore distribution patterns in unsaturated peat soil. The pore–grain interface appears rough, and fractal scaling of soil-pore interfaces has often been found at length scales below the pore size (Schlueter *et al*., 1997), and it is reasonable to expect that the pore surface roughness has some influence on the rate of flow through soils.

In recent years, computer tomographic (CT) imaging (Salem and Chilingarian, 1999) has been used to evaluate the three-dimensional (3D) pore geometry and its role in defining fundamental hydraulic properties of a range of geological materials (Wildenschild *et al*., 2002; Kettridge and Binley, 2008). CT imaging produces a much larger sample size than can be captured on thin sections or blocks, without significantly compromising the image resolution. This method also offers the prospect of examining small-scale soil structures in 3D, and because it is non-destructive, the same sample can be re-scanned for varying moisture conditions (Quinton *et al*., 2009).

The overall objective of this research was to evaluate the effect of porosity, pore shape, pore roughness and tortuosity on the unsaturated hydraulic conductivity of peat soils from different depth positions. This is accomplished via (1) quantifying the detailed air-filled pore size and geometric properties at different depths under a constant soil water pressure head; (2) computing the unsaturated hydraulic conductivity based on pore size and geometry properties; (3) classifying the peat degree of decomposition and compressibility; and (4) examining the factors, obtained from pore size and geometric analysis, controlling the unsaturated hydraulic conductivity under a constant pressure head.

STUDY SITE AND METHODOLOGY

Field sampling and peat core extraction

The *Sphagnum* peat used for this study was collected from an undisturbed peat plateau at Scotty Creek (61°18′N; 121°18′W) in the wetland-dominated zone of a discontinuous permafrost, 55 km south of Fort Simpson, Northwest Territories, Canada. A 20-cm deep peat block with a surface area of 40 × 40 cm was carefully removed from the ground surface of the plateau. A second block was removed from the face of a soil pit at a depth range of 50–70 cm. Both samples were transported to the laboratory, where they were wetted from the bottom-up over a period of 24 h, until they were saturated. They were then transferred to a freezer until they were in a solid state. A hollow drill bit mounted on a drill press was then used to extract four cylindrical cores of 10 cm length and 6 cm diameter at the 0–6, 6–12 and 12–18 cm depths from the upper soil block and 61–67 cm depths from the deeper block. Each subsample core was then weighed and then inserted into a transparent, acrylic, 15-cm long, 6-cm inner diameter tube and allowed to thaw and freely drain under gravity for 48 h. All subsequent measurements were based on the thawed sub-sample cores that remained in these tubes.

Measurements of basic hydraulic and physical properties of peat sub-samples

A constant hydraulic head of −40 cm was maintained for all the sub-samples by setting a head difference between the outflow from the lower disc and the upper disc of a twin pressure plates apparatus constructed from clear Plexiglas (Price *et al*., 2008). Each pressure plate disk was perforated and had 25 μm Nitex fabric glued to it to provide an air entry pressure of about −40 cm, and the other disk was connected to an outflow hose. The twin pressure plates maintained contact with the peat cores at both ends of the peat sub-sample, and the head was set by lowering the hanging columns of water to −40 cm. The unsaturated hydraulic conductivity of peat sub-samples was measured directly using a constant head permeameter technique, based on steady-state flow (Elrick and Reynolds, 1992) and the procedure of Price *et al*. (2008). For this experiment, the volume flux through the unsaturated peat was measured [Q (L^3 T^{-1})]. The unsaturated hydraulic conductivity K [L T^{-1}] was calculated by applying Darcy's law as (Elrick and Bowman, 1964; Price *et al*., 2008):

$$K = \frac{Q}{A(\Delta h/\Delta L)} \tag{1}$$

where A (L^2) is the cross-sectional area of sub-sample (28·3 cm^2), Δh (L) is the head difference across the sub-sample length (2 cm), ΔL (L) is the length of sub-sample and ($\Delta h/\Delta L$) is the hydraulic gradient (0·21).

Basic physical properties of peat soils include the volumetric water content (θ), bulk density (ρ_b), total porosity (ϕ_T) and the degree of decomposition. The sub-samples were weighted at the water pressure −40 cm,

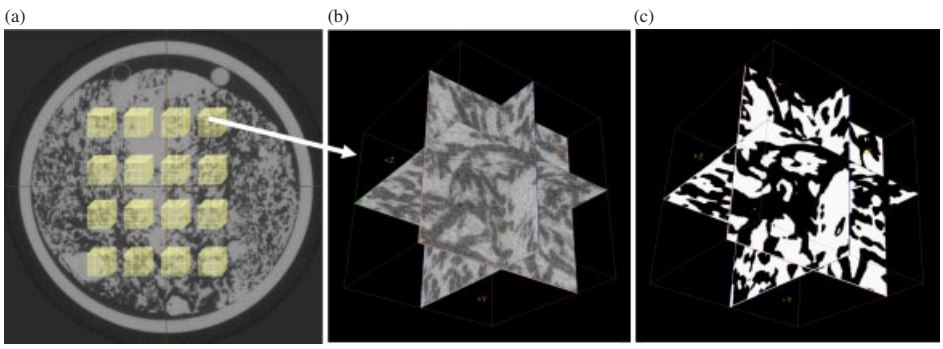

Figure 1. Sample 2D and 3D CT scanning images to visualize the air-filled voids and other solid materials (organic and water) from a sub-sample core. (a) 2D section of greyscale representation of the original acquired image by CT with a size of 1350 × 1350 pixels and position of the 16 regions of interest for scanned sub-sample cores, (b) a 3D visualization of cropped region of the original image with a size of 200 × 200 × 200 voxels and (c) processed binary image of the cropped image (b). Darker colours in the original image show the resin occupying pore spaces and lighter colours show the organic material. In the binary images, black areas represent pores

and the volumetric water content was determined from these values and the same sub-sample volume imaged by the CT scanner (see below) (Gardner, 1986). The bulk densities were calculated on an oven-dry weight basis at 80 °C for a period of 1 week after the scanning was completed; i.e. the ratio of peat oven-dry weight to the unit wet bulk volume. To represent field conditions, the wet bulk volume is used, because when peat materials are dried, their volume is reduced. The total porosity of each sub-sample was gravimetrically determined following the method of Boelter (1976) based on the original sub-sample volume, the sub-sample mass and the dry mass and the volume fraction of air bubbles computed from Quinton *et al*. (2009). The degree of peat decomposition, a key property of organic soil, was measured using the von Post (vP) classification scale (von Post, 1922) with its 10 classes of humification (i.e. H1 referring to undecomposed peat and H10 to highly decomposed peat). The vP scale is based on the colour of the water, structure of the residue and the amount of peat that passes through the fingers when the fresh peat is squeezed (Damman and French, 1987).

3D X-ray CT scanning

After the sub-samples had reached to soil water pressure of −40 cm, they were sealed and equalized with the applied pressure and then moved to an X-ray CT scanner for 3D image acquisition. The sub-samples were scanned at the Department of Land Resource Science, University of Guelph, Canada, using a GE Medical μCT, model MS8X-130, source with 130 kVp monochromatic X-ray beam at 100 kV 80 mA, 3500 ms exposure with a high pass filter to reduce hardening artefacts and enhance contrast between phases. The detector was a high-resolution digital X-ray camera detector system. This detector accumulates all the energy of the transmitted photons and provides the numerical data to be used in reconstructing an image. For each value of hydraulic head, 720 views of the sub-sample were taken at half angle increments over 360°. Each sub-sample was placed vertically within the scanner so that the X-ray intersected the peat core perpendicular to it in the longitudinal axis. A polyethylene sample marker was used to ensure the digital sub-sample was easily re-oriented to correspond with other scans. It was necessary that the sub-sample be oriented vertically to ensure the downward direction of depth. Upon each scan completion, the collected raw data (a series of rotational X-ray images) were reconstructed to a 3D data volume using an ultra-high resolution noise-reducing filtered back-projection algorithm (Wang *et al*., 1993) to derive images with good contrast between the two phases–air-filled pores and the combined water and organic material. The resulting 3D imagery was acquired at size of 1350 × 1350 × 876 voxels in a local 3-D (XYZ) coordinate system with a resolution of 45 × 45 × 45 μm for each voxel. To reduce inherent noise and partial volume effects that are present in X-ray CT data, a noise-reducing homomorphic filter and threshold determination technique were used (Elliot and Heck, 2007). For a more detailed explanation of the methodology, the reader is referred to Rezanezhad *et al*. (2009).

Image analysis and separation of air-filled constituents

Image analysis was carried out by using open source software GE-HC Microview v2.1.1 (http://sourceforge.net/projects/microview) and ImageJ 1·40 g (http://rsbweb.nih.gov/ij/). As the peat soils are strongly anisotropic and heterogeneous (Beckwith *et al*., 2003), 'representative' peat structure needs to be taken from sub-samples. Therefore, to consider the complexity of the general soil structure and the anisotropy, the analyses of 3D images were conducted on the 16 small cropped images from each sub-sample CT image with a sub-volume size of 200 × 200 × 200 voxels (volume of 0·72 cm^3); this resulted in 8 million voxels for each data set. An example of 2D CT image rendering of the pore spaces and selecting the 16 regions of interest is shown in Figure 1a. The distance between the rows in each sub-sample was 1 cm, and each row represents a depth, which includes 4 cropped images. For four scanned sub-samples at different depths, a total of 64 3D images were cropped from the original CT images.

To determine air-filled porosity, the fraction of voids filled with air was calculated from the CT imagery of cropped volume using image segmentation techniques where the air-filled porosity of peat is the ratio of the volume of empty space to the total volume of the cropped image. This determination is crucial, and misinterpretation of the data scalar range can lead to inaccuracies in the imagery due to the sensitivity of image segmentation techniques when investigating materials of similar attenuation (air–water–peat) within X-ray CT imagery. Underestimation or overestimation of air-filled pore space reduces or increases, respectively, the estimate of porosity and blurs or makes erroneous connections between distinct voids.

To achieve an accurate separation of voids from the solid matrix (organic material and water), a new neighbourhood-based standard deviation thresholding algorithm (Elliot and Heck, 2007) was applied to the CT images. This method is based on the range of X-ray linear attenuation coefficient that were expressed in a dimensionless quantity known as Hounsfield units (HU), which relates to the atomic density of materials. The density difference between void (HU $= -1000$) and the remaining constituents of water and organic solids (HU $\approx$0) represented by the non-void voxels allows direct imaging of individual pores and networks. This procedure is a quantitative approach to select a threshold that involves fitting a Gaussian distribution to a bi-modal distribution on a histogram of relative HU density for the sub-sample, wherein the equiprobability point between the bi-modal Gaussian peaks is the threshold that appears to most accurately separate the grey-level classes associated with solids and voids. By applying the derived threshold using ImageJ, the original 16-bit grey-level microtomographic images produce binary imagery after segmentation of the air-filled voids and solid phases, in which void phase voxels are visualized as black and solid phase voxels are white. In this study, the solid and liquid were not separated, as there is at present no effective algorithm that could segment out the organic peat (inclusive of hyaline cells) from the surrounding water with a degree of verisimilitude. Visualization of peat macrovoids or macroporosity in 3D and its binary image are shown in Figure 1b and c. A detailed description of the image processing and thresholding procedure is given in Rezanezhad *et al*. (2009). The threshold value was adjusted for each separate CT scan through this process.

Size and geometric distribution of pores

Because the spatial resolution of the CT scans was sufficiently high, and there was high attenuation contrast between voids and solid material, direct imaging of individual pores and networks was possible. In general, pore space was characterized by low HU, and organic material and water were characterized by relatively high HU. Using 3D digital image analysis techniques, the air-filled pore distribution through peat sub-sample was quantified. The surface area and volume of pores were measured by the latest release of a '3D Objects Counter' algorithm in ImageJ (F. Cordelires, 2008, personal communication). This algorithm provides an accurate segmentation of images into binary values which allow for counting the number of individual pores measurements as well as determining some morphological characteristics (individual pore volume and cross-sectional area, the centre of mass and the centre of intensity) for each separable pore.

Air-filled voids or pores are separated from the rest of image because of the air-filled porosity exclusion principle for flow through the porous material (Winegardner, 1996). We used the 3D Objects Counter algorithm on peat-cropped images at different depths of peat subsamples to identify the physical properties of peat, such as air-filled pore size distribution (porosity), spatial density, and to quantify the tortuosity and 3D hydraulic radius of each individual pores (calculated afterward). The air-filled porosity (ϕ_a) was computed as the total volume of empty pores divided by the total volume of the cropped image from peat sub-sample (V_{img});

$$\phi_a = \sum_i V_i / V_{img}, \tag{2}$$

where V_i (L^3) is the volume of the ith pore on all $200 \times 200 \times 200$ voxels.

To determine an equivalent pore radius for the complex geometries and irregularly shaped pores (Schlueter *et al*., 1997; Rezanezhad *et al*., 2009), which cannot be adequately represented as a spherical or cubic shape, we defined a 3D pore hydraulic radius (R_p) to assess and quantify the geometry of opening surfaces (Milne *et al*., 1996; Wang *et al*., 2007). In this mathematical morphology method, the R_p (L) equals half the maximum harmonic average radius R_{har} (L) of a surface (measured from the centre of the pore surface). The R_{har} is defined as the harmonic average distance from a point on an opening surface to the abutments and expressed as:

$$R_{har} = \frac{1}{\frac{1}{n}\sum_{\theta=1}^{n} 1/r_\theta} \tag{3}$$

where r_θ (L) is the distance from any point on a pore surface to the abutments at angle θ and n is the number of rays measured to the surface edge or abutment. R_{har} has a maximum value towards the centre of the surface for each pore and decreasing values towards the edges. The tortuosity of each pore (τ_p [−]), as one of pore structure descriptor, was calculated as a function of air-filled porosity (Berryman and Blair, 1987):

$$\tau_p = \frac{\phi_a A_p}{\pi R_p^2} \tag{4}$$

where ϕ_a is the air-filled porosity of the cropped volume, A_p is the pore surface area and R_p is the pore hydraulic radius measured for each pores.

Fractal characterization of pores

To describe the fractal dimensions and the effects of pore structure and configuration on flow, the 2D and 3D fractal dimension (D_{2d}, D_{3d}) of the air-filled pore space and solid interface (Mandelbrot, 1983) were measured on CT images. In 2D space, the value of D_{2d} for a set of pores was calculated by the perimeter–area (measured by 'particle analyzer' function in ImageJ) scaling relationship $P = kA^{D_{2d}/2}$, where k is a constant (Mandelbrot, 1983; Schlueter *et al.*, 1997). Euclidian shapes such as squares and circles have a $D_{2d} = 1$, whereas fractal shapes have values of D_{2d} between 1 and 2. In 3D space, the values for D_{3d} lie between 2 and 3, the value being proportional to the apparent roughness of the edge. For 3D fractal dimension, we used ImageJ software, applying the box counting method (Liebovitch and Toth, 1989). In this method, the fractal dimension of an object in 2D image is calculated by using grids of boxes of side length λ overlaid upon an image. Any box containing at least 1 pixel of any part of the structure of the object is considered to bean occupied box. The number of the occupied boxes, N, of side length, λ, is counted. Special care was taken so that none of the pixels in the object are obscured by grid lines. This process is repeated for several values of λ. The 2D box-counting fractal dimension, D_{2d}, can be determined, according to Equation (5), as the negative of the slope of the linear regression curve of the logarithm of the number of occupied boxes N with the side length λ

$$D_{2d} = -\frac{\Delta \ln N}{\Delta \ln \lambda} \tag{5}$$

The value of D_{2d} was calculated for each 2D slice, separately measuring the edge of each pore for all pores in each slice. The fractal dimension in 3D space is obtained by averaging the fractal dimensions obtained from each 2D slice of single images and adding 1, assuming isotropic structure of the 2D slices (Mandelbrot, 1983; Dathe *et al.*, 2001; Tang and Marangoni, 2006).

Unsaturated K estimates based on pore size distribution

We used the modified Kozeny–Carman expression from Rezanezhad *et al.* (2009) to compute the permeability of each sub-sample:

$$K_p^* = c\frac{\left(R' - R_p\right)^2 (\phi_T - \phi_a)^3}{(1 - (\phi_T - \phi_a))^2} \tag{6}$$

where K_p^* is the unsaturated pore permeability, c is the pore shape coefficient, R_p is the pore radius factor, ϕ_a is the air-filled porosity, ϕ_T is the total porosity and R' is the maximum water-filled radius factor of largest pore, measured at a soil water pressure of −40 cm. The pore shape coefficient c is known to be controlled by flowpath tortuosity, the number and sphericity of pores, and other shape factors that affect flow (Freeze and Cherry, 1979), and is computed from:

$$c = \left(\frac{S_p}{N^2 \times \tau_p}\right) \tag{7}$$

where S_p [−] is the pore sphericity, N is the number of air-filled pores and τ_p [−] is the pore path tortuosity [Equation (4)]. The S_p can be calculated by:

$$S_p = \frac{\pi^{1/3}(6V_p)^{2/3}}{A_p} \tag{8}$$

where V_p and A_p are the pore volume and surface area, respectively (Wadell, 1935). The average intrinsic permeability of total pores was used to estimate the unsaturated hydraulic conductivity, K, using equation (Freeze and Cherry, 1979, p. 27);

$$K = K^*\frac{\rho g}{\mu}, \tag{9}$$

where K^* (L^2) is the average intrinsic permeability of total pores, ρ (M L^{-3}) is the water density, g [9·8 L T^{-2}] is gravitational acceleration and μ (M L^{-1} T^{-1}) is the dynamic viscosity of the water.

RESULTS AND DISCUSSION

Table I lists the measured physical and hydraulic properties of sub-samples at four depths. Volumetric water content at a pressure head of −40 cm increased from 0·38 to 0·43 cm^3/cm^3 with increasing depth. The measured bulk density of peat sub-samples varied from 0·035 to 0·115 g/cm^3 corresponding to an increase in the degree of peat decomposition from class H2 (poorly decomposed) to H5 (moderately decomposed). The unsaturated hydraulic conductivity measured using the permeameter-based method showed a decrease with depth from $4{\cdot}0 \times 10^{-6}$ m/s near the ground surface to $4{\cdot}7 \times 10^{-7}$ m/s at depth 61–67 cm.

Quantification of size and geometric properties of pores

At a soil water pressure of −40 cm, most of the inter-particle space is air filled and the air-filled porosity is essentially the active porosity (Quinton *et al.*, 2009; Rezanezhad *et al.*, 2009), as the total porosity of the peat includes the volume fraction of the relatively large, inter-particle pores that actively transmit water (active porosity) and the relatively small, closed and dead-end pores formed by the remains of plant cells (inactive porosity) (Hoag and Price, 1997). An average air-filled porosity

Table I. Measured physical and hydraulic properties of sub-sampled peat by depth: the total porosity (ϕ_T), water content (θ), bulk density (ρ_b), von Post scale (vP) and unsaturated hydraulic conductivity (K) measured by permeameter method, all at a pressure head of −40 cm

Sub-sample	Depth (cm)	ϕ_T (%)	θ (cm^3/cm^3)	ρ_b (g/cm^3)	vP (−)	K (m/s)
S(I)	0–6	0.95	0.38	0.035	H2	4×10^{-6}
S(II)	6–12	0.86	0.42	0.054	H3	2×10^{-6}
S(III)	12–18	0.93	0.40	0.071	H3	$5{\cdot}7 \times 10^{-7}$
S(IV)	61–67	0.92	0.43	0.115	H5	$4{\cdot}7 \times 10^{-7}$

Table II. Summary results of physical and hydraulic properties analysis of 3D cropped images from the sub-samples at 16 depths below ground surface: the air-filled porosity (ϕ_a), density or number of the air-filled pores per cm^3, average pores tortuosity ($\overline{\tau}_p$), mean 3D hydraulic radius (R), 3D fractal dimension (D_{3d}), computed unsaturated hydraulic conductivity (K). The cropped image volume from sub-sample was 0·72 cm^3 (200 × 200 × 200 voxels)

Sub-sample	Depth (cm)	ϕ_a (%)	Density (per cm^3)	$\overline{\tau}_p$ (−)	R (cm)	D_{3d} (−)	K (m/s)
S(I)	3	45·9	79	4·93	0·0122	2·71	$7{\cdot}9 \times 10^{-5}$
	4	52·9	45	3·68	0·0128	2·7	$5{\cdot}6 \times 10^{-5}$
	5	53·5	70	4·50	0·009	2·68	$1{\cdot}2 \times 10^{-5}$
	6	47·3	86	4·51	0·0099	2·69	$1{\cdot}3 \times 10^{-5}$
S(II)	7	51·1	70	3·79	0·0088	2·69	$3{\cdot}6 \times 10^{-6}$
	8	51·4	85	4·45	0·0088	2·75	$2{\cdot}7 \times 10^{-6}$
	9	56·4	121	5·15	0·0082	2·67	$1{\cdot}8 \times 10^{-6}$
	10	43·1	150	3·92	0·0072	2·68	$2{\cdot}2 \times 10^{-6}$
S(III)	12·5	56·5	116	5·03	0·0086	2·67	$3{\cdot}3 \times 10^{-6}$
	13·5	50·1	122	4·47	0·0082	2·67	$3{\cdot}4 \times 10^{-6}$
	14·5	47·9	143	4·34	0·0077	2·65	$3{\cdot}4 \times 10^{-6}$
	15·5	61·6	73	4·92	0·0092	2·64	$1{\cdot}6 \times 10^{-6}$
S(IV)	62	49·2	328	6·9	0·0053	2·30	$4{\cdot}6 \times 10^{-7}$
	63	56·7	339	6·00	0·0063	2·32	3×10^{-7}
	64	50·8	278	6·15	0·0056	2·30	$5{\cdot}2 \times 10^{-7}$
	65	51·8	402	7·31	0·0057	2·30	$4{\cdot}8 \times 10^{-7}$

of approximately 50, 51, 54 and 52% (Table II) for the sub-samples S(I), S(II), S(III) and S(IV), respectively, is reasonable, given that the difference between it and the measured total porosity of ∼95, 86, 93 and 92% (Table I) is accounted for by the sum of the inactive porosity, which is typically ∼20% (Hoag and Price, 1997); and a residual of ∼20% that would be accommodated in the sample at the −40 cm by the water held in the remaining films and the volume fraction of air bubbles (∼11%, reported by Quinton *et al*., 2009).

The summary results of morphometric analysis obtained from 64 3D CT scanning images at 16 different depths below ground surface are listed in Table II (the mean values of all four measurements at each depth from the surface were then averaged). The vertical distribution of air-filled porosity shows little variability (the ranges of minimum and maximum measured values for each depth are shown in Figure 2a). There was an increase in the number of air-filled pores with increasing depth (Figure 2b). Although there were no important changes in total air-filled pore space with depth, important changes in pore size were observed. The pore size range for individual sub-samples was variable, and there was a general decrease in the average hydraulic radius of pores (Figure 2c) and increase in the average pore tortuosity (Figure 2d) with respect to peat depth below ground surface. The mean hydraulic radius of pores at upper depths was 0·012 cm and then decreased to about 0·005 cm at ∼60 cm.

Estimation of unsaturated hydraulic conductivity

The unsaturated hydraulic conductivity values computed from Equation (9) matched closely with the values measured using the permeameter (Tables I and II). Equations (6)–(8) indicate that a change in the number, volume and tortuosity of air-filled pores affects the permeability of peat. Differences in pore size distribution of the various depths resulted in striking differences in the unsaturated hydraulic conductivity (Table II). As depth increases, the number of pores and the tortuosity increase, whereas the pore hydraulic radius decreases, and as a result the hydraulic conductivity decreases. Unsaturated hydraulic conductivity decreased by more than an order of magnitude between the 0 and 15 cm depth ($7{\cdot}9 \times 10^{-5}$ to $1{\cdot}6 \times 10^{-6}$ m/s) and then decreased by about three times to $4{\cdot}8 \times 10^{-7}$ m/s between 15 and 62 cm and remained nearly constant below 60 cm depth (Figure 3), which corresponds approximately with the interface between the lightly decomposed upper peat depth and the more heavily decomposed lower depth.

This large reduction of unsaturated hydraulic conductivity with depth (Figure 3) is most likely governed by the reduction in the geometry and the size of individual air-filled pores (Table II) due to degree of decomposition and compression of the organic matter, even though the air-filled porosity and water content of peat do not vary appreciably within the 0–67 cm depth range (Tables I and II) at an applied constant pressure head of −40 cm. Therefore, the differences are related to the degree of decomposition and compressibility characteristics, which largely determines the porosity and pore size distribution. In the following, we will try to explain how hydraulic conductivity may be influenced by the pore size and geometry, measured from the 3D CT digital images.

Peat decomposition and compressibility

The degree of decomposition of peat at the sampled depths used in this study is presented in Table I using the von Post (vP) classification scale. The upper depth of peat was relatively poorly decomposed with vP of H3 and the vP of the lower depth was H5 indicating moderately decomposed peat. The distribution of air-filled pores and other materials for two sub-sample cores at two different depths (0–6 and 61–67 cm) is

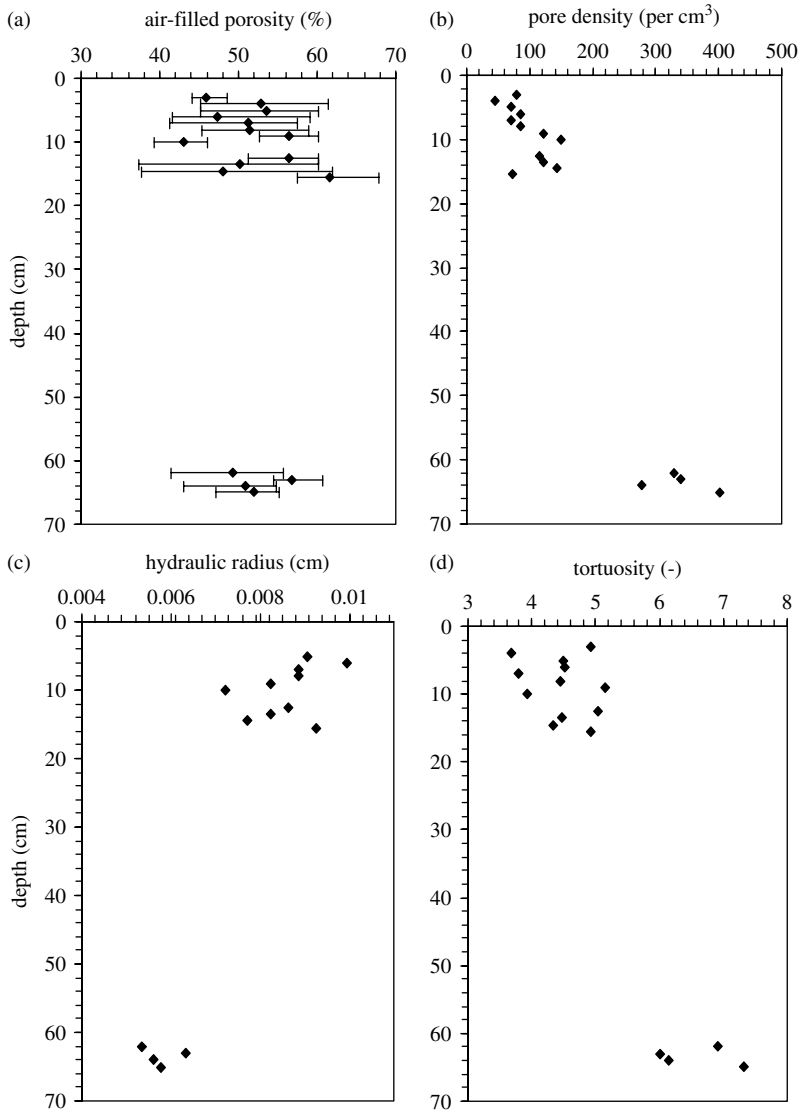

Figure 2. Variations in (a) air-filled porosity, (b) density, (c) hydraulic radius and (d) tortuosity with respect to peat depth below ground surface for 16 different depths at a constant pressure head (−40 cm)

illustrated using 2D CT scanning image in Figure 4. This figure shows that the peat soil consisted of different structural arrangements with an increase in depth. The upper peat depths (Figure 4a) were a relatively porous layer composed of large, angular aggregated pores (black area in binary image). In comparison, the lower depth was a denser (Figure 4b) solid matrix including the organic material and water (white area in binary image) with high proportion of smaller pores.

Visualization of air-filled pores in peat at various depths portrayed in a 3D isosurface map (Figure 5) illustrates their size distribution, structural discontinuity and geometry. As suggested in Figure 5, quantified 3D CT data indicated that at the constant pressure head (−40 cm) applied for the sub-samples, there are significantly more distinct, yet volumetrically smaller air-filled pores with increased depth. Therefore, as compression proceeds, the size of organic particles decreases, resulting in smaller pores and higher bulk density. In this study, geometry properties of peat pores (hydraulic radius and fractal dimension) at different depths were assessed to determine whether they can be used as indicator of peat compressibility.

Factors controlling the flow through unsaturated peat

In addition to the gradient of pressure head, the rate of flow through unsaturated peat depends on the hydraulic conductivity of the peat, which is a function of the water content and the structure, distribution, size and geometry of pores (Rezanezhad *et al*., 2009). The hydraulic conductivity of *Sphagnum* peat decreases sharply upon drainage, because it loses a large portion of its saturated water content at suctions of only −2 cm (Price *et al*., 2008; Rezanezhad *et al*., 2009). Price *et al*. (2008) found that for poorly decomposed hummock mosses at a given pressure, the deeper samples had higher water retention, thus higher unsaturated hydraulic conductivity. In contrast, the water content and air-filled porosity of the peat examined in this study did not vary substantially with depth (Tables I and II) at a constant

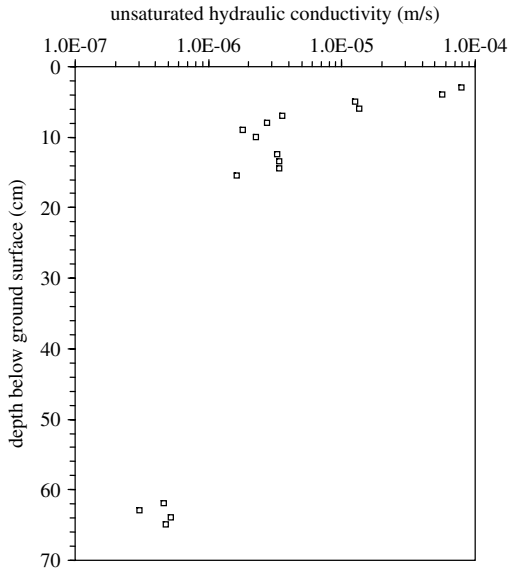

Figure 3. Unsaturated hydraulic conductivity of peat under a constant pressure head (−40 cm) computed for all the 64 cropped images, where each symbol represents an average value of four measuring cropped images at each depth from the surface. This was done by computing the permeability using Equation (6) and then converting the permeability values to unsaturated hydraulic conductivity through Equation (9). Unsaturated hydraulic conductivity, K, varies by over two orders of magnitude with depth in the peat profile

pressure head (−40 cm), so the decrease in unsaturated hydraulic conductivity with depth was a function of the increased tortuosity (Figure 2d) arising from the smaller pore size and altered geometry of the air-filled pores in deeper peat (Table II).

Tortuosity is one of the most meaningful 3D parameters of pore structure, which expresses the degree of complexity of the sinuous pore path. This factor is based on the fact that pores are irregular and upon drying, water will concentrate in small angles and crevices of the pore system as water films. Tortuosity can easily be related to the hydraulic conductivity of a porous medium because it provides an indication of increased resistance to flow due to the greater path length of the pore system; i.e. an increased path length results less connection or reducing the hydraulic conductivity (Dullien, 1979; Vogel, 1997). The connectivity of the pore space plays an important role in soil hydraulic properties and in its hysteretic behaviour; however, a quantitative morphological description of the connectivity of the complex porous structure in peat soil is difficult.

Examples of complexity of the edge of the pores in 2D are shown in Figure 6a–d. The fractal dimension, D_{2d}, was used to characterize the irregularity or roughness of surfaces. Figure 6 (right) shows the logarithmic plotting of the perimeter against the area of pores. The straight line best fitting the points indicates fractal scaling in 2D. The slope of this line ($D_{2d}/2 = \log(P)/\log(A)$), multiplied by 2, is the fractal dimension ($D_{2d} = 1{\cdot}22$). We also compared 3D fractal dimensions and looked

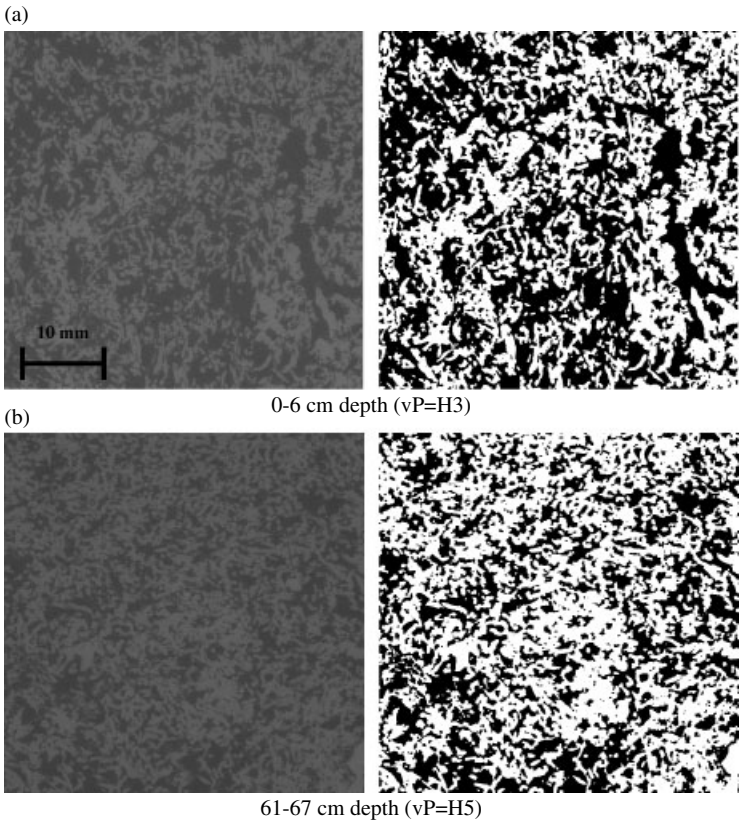

Figure 4. Sample 2D section of CT scanning image to visualize the air-filled pore space and solid materials with a size of 900 × 900 pixels (∼40 × 40 mm), showing the degree of decomposition at two different depths: (a) 0–6 cm and (b) 61–67 cm sub-samples in this study. The dark area in original acquired images (left) and black area in processed binary images (right) represent the air-filled pore spaces and the light and white areas represent the water plus organic material spaces. The vP is von Post classification scale indicating degree of decomposition

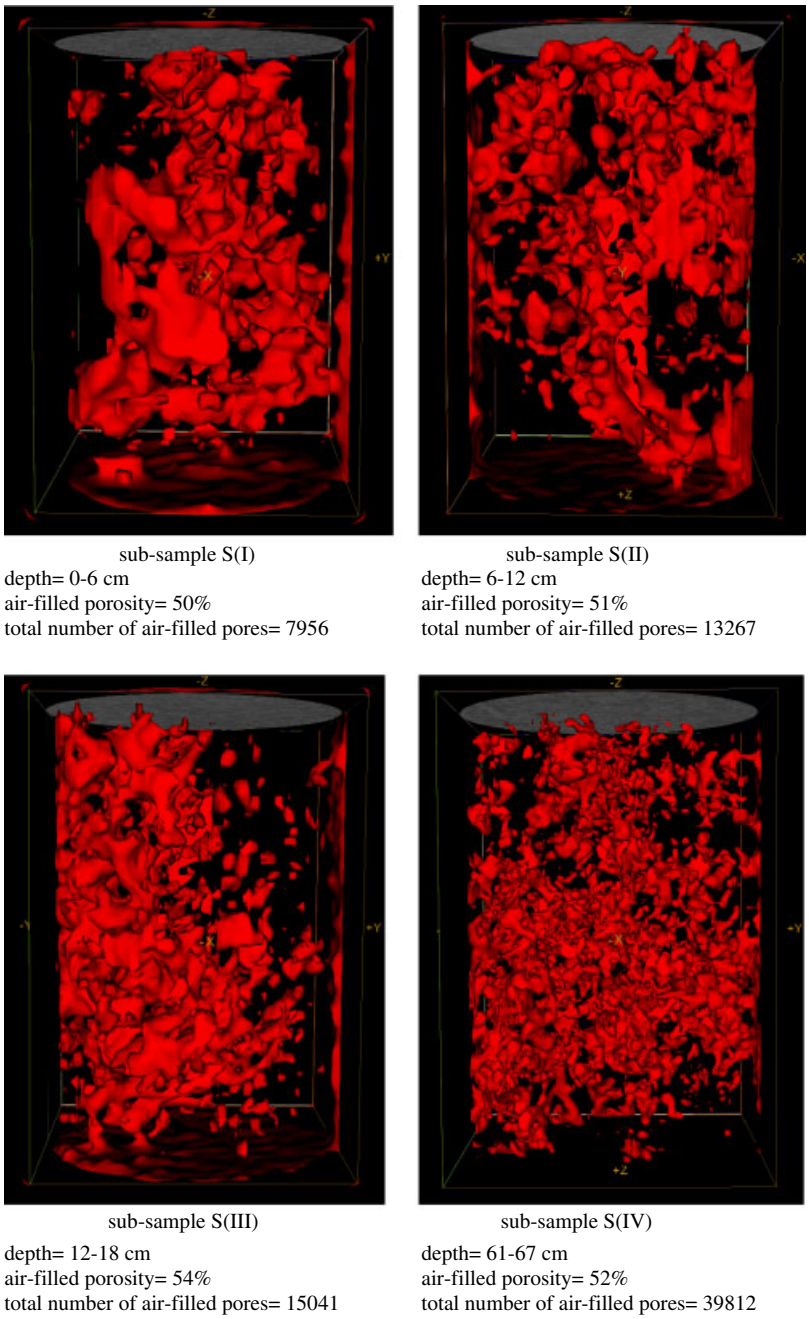

Figure 5. 3D isosurface image visualization of the air-filled pores for the four drained peat sub-sample cores extracted from the four different depths with size of 1325 × 1225 × 824 voxels. Red colours in the images show the air-filled pores

for correlations between the fractal dimensions and some characteristics of the peat soils at different depths. The results of calculated 3D fractal dimensions of the air-filled pores for all the 16 depths are shown in Table II, and the correlations between the fractal dimensions and depth of sub-sampled peats are plotted in Figure 7. The mean fractal dimension of 16 cropped peat volumes varies with depth with extreme values of $2{\cdot}7 \pm 0{\cdot}054$ for the upper depth (poorly decomposed) to $2{\cdot}3 \pm 0{\cdot}048$ for the lower depth (moderately decomposed), indicating that the pores are getting irregular with lower surface roughness at lower depth. These results indicate how the pore structure and configuration affect the flow. When the air-filled pores at lower depths are smaller and irregular with lower surface roughness, the water concentrates in small angles and flow occurs along path length within water films on the surface. Therefore, these irregular air-filled pores contribute to the obstruction of flow and reduce the unsaturated hydraulic conductivity. Because the fractal dimension quantifies the structure and configuration of the pore surfaces, it is reasonable to expect that it is related to the rate of flow through porous media. The correlation between both fractal dimensions and tortuosity with unsaturated peat hydraulic conductivity is shown in Figure 8 for the 16 cropped volumes of peat at different depths.

Another relevant parameter affecting hydraulic conductivity is the hydraulic radius of the air-filled pores. As

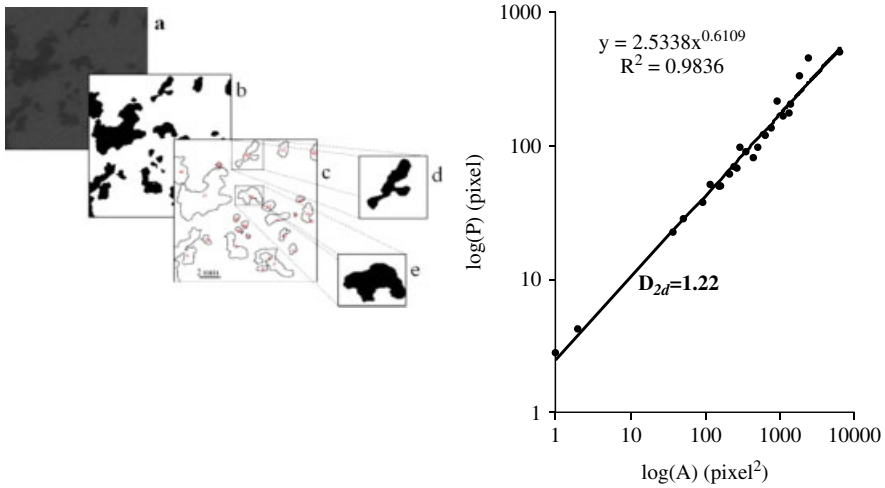

Figure 6. Left: (a) 8-bit grey-level image of sub-sample with a cross-section area of 288 × 314 pixel, (b) binary image, (c) counted pores by particle analyzer and (d, e) fractal shape of pores. Right: log–log plot of pore perimeter P and area A, which determine the 2D fractal dimension of the pores in a 2D representation of the sub-sample

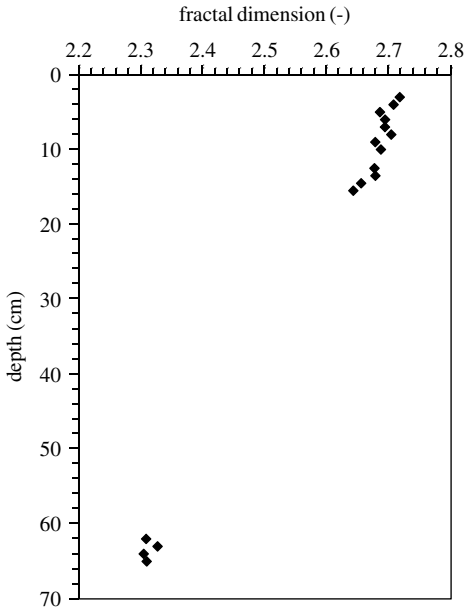

Figure 7. Correlation between 3D fractal dimensions (D_{3d}) of the air-filled pores obtained using box-counting method and depth for all the 64 cropped images, where each symbol represents an average value of four measuring cropped images at each depth from the surface

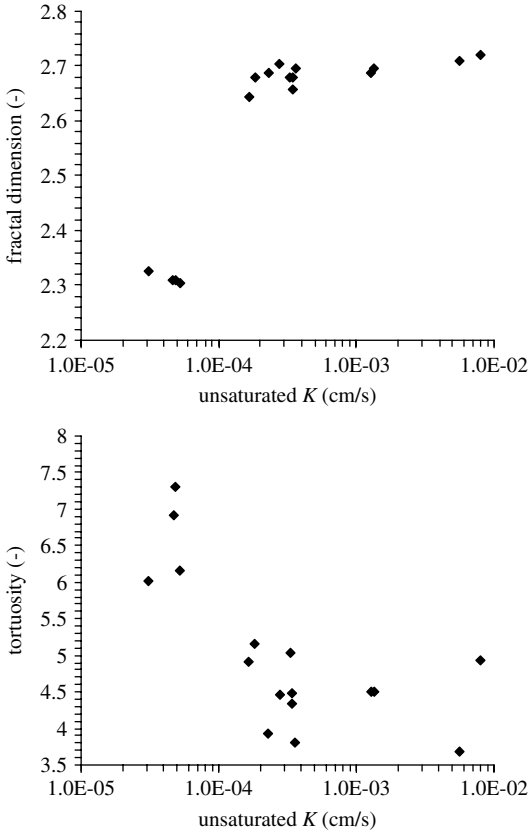

Figure 8. Relationships between the tortuosity parameter and the pore-related structural parameter of 3D fractal dimension with the computed unsaturated hydraulic conductivity, indicating decreasing unsaturated hydraulic conductivity with increasing mean tortuosity and decreasing mean fractal dimension

the more decomposed peat materials at lower depths have more small air-filled pores (i.e. increasing pore density), the hydraulic radius decreases and hence the tortuosity of peat materials increases with increasing degree of decomposition, indicating that sub-samples with small number and larger air-filled pores would have shorter path lengths (Table II).

SUMMARY AND CONCLUSIONS

The hydraulic properties of unsaturated peat are controlled by the peat structure and air-filled pore size and geometric distribution as well as the physical properties of peat materials. *Sphagnum* peats showed changes in their physical properties such as degree of peat decomposition and compression that directly affect its hydraulic properties. The modified Kozeny–Carman Equation (6) was used to compute the unsaturated hydraulic conductivity, which expresses a strong dependence of permeability on the hydraulic pore radius R, the pore shape coefficient c, the pore tortuosity τ_p and the porosity ϕ. The computed

unsaturated hydraulic conductivity showed more than an order of magnitude decrease with depth from $7{\cdot}9 \times 10^{-5}$ m/s near the ground surface to $4{\cdot}8 \times 10^{-7}$ m/s at depth 65 cm. Estimates of unsaturated hydraulic conductivities were made for the purpose of testing the sensitivity of pore shape and geometry parameters on the hydraulic properties of peats and how to evaluate the structure of the peat and its effects on parameterization.

Based on pore geometry information obtained from image analysis, the fractal dimension was calculated for the pore space structure and its influence on peat unsaturated hydraulic conductivity. These values showed how the pore structure and configuration affect the flow. The air-filled pores at lower depths are smaller, irregular with lower surface roughness, higher tortuosity and lower connectivity. Therefore, this research showed increasing peat pore configuration at lower depths delayed water flow and reduced the unsaturated hydraulic conductivity. Conceptually, a relationship between these parameters of peat materials makes sense. The hydraulic conductivity of peat decreases with increasing degree of decomposition and/or compression because these factors breakdown the peat structure. This produces smaller fibres that are packed more tightly and as such are more able to resist flow through the inter-particle spaces.

Three-dimensional CT digital image analysis of peat samples showed that the pore structure and configuration of peat soils are very complex and contains many variables in its physical and hydraulic properties at different depths. This study suggests that large reduction of unsaturated hydraulic conductivity with depth, under a constant pressure head, is controlled by air-filled pore hydraulic radius, tortuosity, air-filled pore density and the fractal dimension due to degree of decomposition and compression of the organic matter. Quantified 3D CT data indicated that at the constant pressure head (-40 cm), there are significantly more distinct, yet volumetrically smaller air-filled pores with increased depth. At lower peat depths, where the air-filled pores are smaller with lower surface roughness, water concentrates in small angles and crevices of the pore system as water films with a path length. These irregular air-filled pores contribute to the obstruction of flow and reduce the unsaturated hydraulic conductivity significantly at lower depths. The improved understanding of the effect of porosity, pore shape, pore roughness and tortuosity on the unsaturated hydraulic conductivity of peat soils increases the capacity to simulate and predict changes in moisture and gas fluxes to the atmosphere in response to natural or human disturbance to peat surfaces.

ACKNOWLEDGEMENTS

Funding for this project was provided by the Canadian Foundation for Climate and Atmospheric Sciences (IP3 Research Network), the Natural Sciences and Engineering Research Council and the International Polar Year. The authors thank Mr P. Whittington and Mr T. Myers for their assistance in obtaining peat samples in the field and laboratory measurements. We thank Dr Richard Heck (University of Guelph, Land Resources Science Department) for the permission to use the CT scanner at the Department of Land Resources Science, University of Guelph. We gratefully acknowledge the Aurora Research Institute for their assistance in obtaining a research license (#13786). We also wish to thank the Jean-Marie River First Nation, the Denedeh Resources Committee, Deh Cho First Nation, Fort Simpson Métis Local #52, Liidlii Kue First Nation and the Village of Fort Simpson for their support of this project.

REFERENCES

Beckwith CW, Baird AJ, Heathwaite AL. 2003. Anisotropy and depth-related heterogeneity of hydraulic conductivity in a bog peat. I: laboratory measurements. *Hydrological Processes* **17**: 89–101.

Berryman JG, Blair SC. 1987. Kozeny-Carman relations and image processing methods for estimating Darcy's constant. *Journal of Applied Physics* **63**: 2221–2228.

Boelter DH. 1965. Hydraulic counductivity of peats. *Soil Science* **100**(4): 606–609.

Boelter DH. 1968. Important physical properties of peat materials. *Proceedings of the 3rd International Peat Congress*, Quebec; 150–154.

Boelter DH. 1976. Methods for analysing the hydrological characteristics of organic soils in marsh-ridden areas. In *Hydrology of Marsh-Ridden Areas, Proceedings of IASH Symposium Minsk., 1972*, IASH, UNESCO, Paris; 161–169.

Carey SK, Woo M-K. 2001. Slope runoff processes and flow generation in a subarctic, subalpine environment. *Journal of Hydrology* **253**: 110–129.

Cohen MH. 1987. In *Physics and Chemistry of Porous Media*, Banaver JR, Koplik J Winkler KW (eds). AIP Conf. Proc. No. 154, American Institute of Physics: New York; p. 3.

Colley BE. 1950. Construction of highways over peat and muck areas. *American highways* **29**(1): 3–6.

Damman AWH, French TW. 1987. The ecology of peat bogs of the glaciated northeastern United States: a community profile. *U.S. Fish & Wildlife Service Biological Report* **85**(7): 100.

Dathe A, Eins S, Niemeyer J, Gerold G. 2001. The surface fractal dimension of the soil-pore interface as measured by image analysis. *Geoderma* **103**: 203–229.

Dullien FAL. 1979. *Porous Media-Flow Transport and Pore Structure*, 2nd edn. Academic press: New York.

Elliot TR, Heck RJ. 2007. A comparison between 2D vs 3D thresholding of X-ray CT imagery. *Canadian Journal of Soil Science* **84**(4): 405–412.

Elrick DE, Bowman DH. 1964. Note on an improved apparatus for soil moisture flow measurements. *Proceedings of the Soil Science Society of America* **28**: 450–453.

Elrick DE, Reynolds WD. 1992. Infiltration from constant-head well permeameters and infiltrometers. In *Advances in Measurement of Soil Physical Properties: Bringing Theory into Practice*, Topp GC, Reynolds WD, Green RE (eds). Soil Science Society of America: Madison, WI, Special Publication no. 30; 1–24.

Freeze RA, Cherry JA. 1979. *Groundwater*. Prentice-Hall: Englewood Cliffs, NJ; 604.

Gardner WH. 1986. Water content. In *Methods of Soil Analysis: Physical and Mineralogical Methods, Agronomy Series 9 (Part 1)*, Kiute A (ed.). Soil Science Society of America: Madison, Wisconsin; 493–544.

Hayward PM, Clymo RS. 1982. Profiles of water content and pore size in *Sphagnum* peat, and their relation to peat bog ecology. *Proceedings of the Royal Society of London, Series B* **215**: 299–325.

Hoag RS, Price JS. 1995. A field-scale, natural gradient solute transport experiment in peat at a Newfoundland blanket bog. *Journal of Hydrology* **172**: 171–184.

Hoag RS, Price JS. 1997. The effects of matrix diffusion on solute transport and retardation in undisturbed peat in laboratory columns. *Journal of Contaminant Hydrology* **28**: 193–205.

Hobbs NB. 1986. Mire morphology and the properties and behaviour of some British and foreign peats. *Quarterly Journal of Engineering Geology* **19**: 7–80.

Karamanev DG, Belanger M-C, Chavarie C, Chaouki J, Talbot P, Mayer R. 1994. Hydrodynamic characteristics of a trickling bed of peat moss used for biofiltration of wastewater. *The Canadian Journal of Chemical Engineering* **72**: 411–417.

Kettridge N, Binley A. 2008. X-ray computed tomography of peat soils: measuring gas content and peat structure. *Hydrological Processes* **22**: 4827–4837. DOI: 10.1002/hyp.7097.

Liebovitch LS, Toth TI. 1989. A fast algorithm to determine fractal dimensions by box counting. *Physics Letters A* **141**: 386–390.

Mandelbrot BB. 1983. *The Fractal Geometry of Nature*. Freeman & Co: New York.

Milne DM, Pakalnis RC, Lunder PJ. 1996. Approach to the quantification of hanging wall behaviour. *Transactions of the Institution of Mining and Metallurgy* **105**: A69–A74.

Price JS, Schlotzhauer SM. 1999. Importance of shrinkage and compression in determining water storage changes in peat: the case of a mined peatland. *Hydrological Processes* **13**: 2591–2601.

Price JS, Whittington PN. 2010. Water flow in *Sphagnum* hummocks: mesocosm measurements and modeling. *Journal of Hydrology* **381**(3–4): 333–340.

Price JS, Cagampan J, Kellner E. 2005. Assessment of peat compressibility: is there an easy way?. *Hydrological Processes* **19**: 3469–3475.

Price JS, Whittington PN, Elrick DE, Strack M, Brunet N, Faux E. 2008. A method to determine unsaturated hydraulic conductivity in living and undecomposed *Sphagnum* moss. *Soil Science Society of America Journal* **15**: 487–491.

Quinton WL, Marsh P. 1999. A conceptual framework for runoff generation in a permafrost environment. *Hydrological Process* **13**: 2563–2581.

Quinton WL, Gray DM, Marsh P. 2000. Subsurface drainage from hummock-covered hillslope in the Arctic tundra. *Journal of Hydrology* **237**: 113–125.

Quinton WL, Hayashi M, Carey SK. 2008. Peat hydraulic conductivity in cold regions and its relation to pore size and geometry. *Hydrological Processes* **22**(15): 2829–2837.

Quinton WL, Elliot T, Price JS, Rezanezhad F, Heck R. 2009. Measuring physical and hydraulic properties of peat from X-ray tomography. *Geoderma* **153**: 269–277.

Rezanezhad F, Quinton WL, Price JS, Elrick D, Elliot TR, Heck RJ. 2009. Examining the effect of pore size distribution and shape on flow through unsaturated peat using 3-D computed tomography. *Hydrology and Earth System Sciences* **13**: 1993–2002.

Salem HS, and Chilingarian GV. 1999. Determination of specific surface area and mean grain size from well-log data and their influence on the physical behavior of offshore reservoirs. *Journal of Petroleum Science and Engineering* **22**: 241–252.

Schlueter EM, Zimmerman RW, Witherspoon PA, Cook NGW. 1997. The fractal dimension of pores in sedimentary rocks and its influence on permeability. *Engineering Geology* **48**: 199–215.

Strack M, Price JS. 2009. Moisture controls on carbon dioxide dynamics of peat-*Sphagnum* monoliths. *Ecohydrology* **2**(1): 34–41.

Tang D, Marangoni A. 2006. 3D fractal dimension of fat crystal networks. *Chemical Physics Letters* **433**: 248–252.

Vogel HJ. 1997. Morphological determination of pore connectivity as a function of pore size using serial sections. *European Journal of Soil Science* **48**: 365–377.

Von Post L. 1922. Swedish geological peat survey with the results obtained so far (in Swedish). *Svenska Mosskulturföreningens tidskrift* **36**: 1–27.

Waddington JM, Quinton WL, Price JS, Lafleur P. 2009. Advances in Canadian peatland hydrology, 2003–2007. *Canadian Water Resources Journal* **34**(2): 139–148.

Wadell H. 1935. Volume, shape and roundness of quartz particles. *Journal of Geology* **43**: 250–280.

Wang G, Lin TH, Cheng PC, Shinozaki DM. 1993. A general cone-beam reconstruction algorithm. *IEEE Transactions on Medical Imaging* **12**(3): 486–496.

Wang J, Milne D, Wegner L, Reeves M. 2007. Numerical evaluation of the effects of stress and excavation surface geometry on the zone of relaxation around open stope hanging walls. *International Journal of Rock Mechanics and Mining Sciences* **44**(2): 289–298.

Wildenschild D, Hopmans JW, Vaz CMP, Rivers ML, Rikard D, Christensen BSB. 2002. Using X-ray computed tomography in hydrology: systems, resolutions, and limitations. *Journal of Hydrology* **267**: 285–297.

Winegardner DL. 1996. *An Introduction to SOILS for Environmental Professionals*. CRC Press, Inc., Lewis Publishers, Corporate Blvd. 2000: Boca Raton, Florida 270pp.

Wong PZ, Howard J, Lin JS. 1986. Surface roughening and the fractal nature of rocks. *Physical Review Letters* **57**(5): 637–640.

Xu Y. 2004. Calculation of unsaturated hydraulic conductivity using a fractal model for the pore-size distribution. *Computers and Geotechnics* **31**(7): 549–557.

Xu YF, Sun DA. 2002. A fractal model for soil pores and its application to determination of water permeability. *Physica A* **316**: 56–64.

